Available online at www.sciencedirect.com
SCIENCE DIRECT®
Microporous and Mesoporous Materials 84 (2005) 179–191
MICROPOROUS AND MESOPOROUS MATERIALS
www.elsevier.com/locate/micromeso

Entropy effects in adsorption and diffusion of alkane isomers in mordenite: An investigation using CBMC and MD simulations

J.M. van Baten, R. Krishna *

Van 't Hoff Institute for Molecular Sciences, University of Amsterdam, Nieuwe Achtergracht 166, 1018 WV Amsterdam, The Netherlands

Received 3 March 2005; received in revised form 5 May 2005; accepted 9 May 2005
Available online 28 June 2005

Abstract

Configurational-bias Monte Carlo (CBMC) simulations were carried out to determine the sorption isotherms for hexane isomers (*n*-hexane, 2-methylpentane and 2,2-dimethylbutane) and butane isomers (*n*-butane and iso-butane) in MOR zeolite. The hexane and butane isomers adsorb exclusively within the 12-ring channels. For a given carbon number, the sorption strength, and capacity, increases with the degree of branching. This is due to the increased packing efficiency within the one-dimensional 12-ring channels when the degree of branching increases. Molecular dynamics (MD) simulations were performed to determine both the Maxwell–Stefan (M–S) diffusivities $Đ_i$, and the self-diffusivities, $D_{i,\text{self}}$, of pure components and mixtures, for a range of molecular loadings. Diffusion was found to be uni-dimensional, and no single file diffusion behavior is observed. Entropy effects cause a reversal in the hierarchy of diffusivity values at high loadings. For example, at low loadings the more compact 22DMB diffuses slower than the slimmer nC6 molecule, whereas at high loadings the reverse is true. The diffusion in mixtures of alkane isomers could be predicted very well by the Maxwell–Stefan diffusion formulation, using only pure component adsorption and diffusion data. In these predictions the Reed–Ehrlich model is used to describe the loading dependence of the pure component M–S diffusivities $Đ_i$. Furthermore, correlation effects are described by self-exchange coefficients $Đ_{ii}$, obtained from fitting the pure-component diffusion data. The special features of adsorption and diffusion in one dimensional zeolite topologies are emphasized by comparison with simulations in FAU and MFI zeolites.

Keywords: MOR zeolite; Multicomponent diffusion; Alkane mixtures; Single file diffusion; Maxwell–Stefan diffusion; Molecular dynamics; Configurational-bias Monte Carlo simulations

1. Introduction

Due to its high thermal stability, mordenite has been used as a catalyst for important reactions such as hydrocracking, hydroisomerization, alkylation, transalkylation, reforming, cracking, dewaxing, and the production of dimethylamines [1–3]. Mordenite has also been used in the adsorptive separation of gas or liquid mixtures [4], and in membrane separations [5,6]. In addition, mordenite has been considered for applications in semiconductors, chemical sensors, and non-linear optics [7]. MOR zeolite is uni-dimensional; it has 12-ring channels and 8-ring side pockets interspaced along these channels. Adsorbates can only move in the *z*-direction, as opposed to three-dimensional transport as in the case of FAU, LTA and MFI zeolites, for example. Catalytic conversions and separation selectivities are often crucially dependent on the adsorption and diffusion properties of molecules within the one-dimensional channels of MOR and there have been some experimental [8,9] and theoretical investigations [10–12] of these properties. Recent work using configurational-bias Monte Carlo (CBMC) simulations have emphasized that entropy, or packing efficiency effects, have significant influence on the adsorption of alkane isomers in one-dimensional

* Corresponding author. Tel.: +31 20 525 7007; fax: +31 20 525 5604.
E-mail address: r.krishna@uva.nl (R. Krishna).

1387-1811/$ - see front matter © 2005 Elsevier Inc. All rights reserved.
doi:10.1016/j.micromeso.2005.05.025

Nomenclature

a_i	constants describing self-exchange, dimensionless
b_i	constants describing self-exchange, dimensionless
b_A, b_B	constants in the dual-site Langmuir model fits, dimensionless
$[B]$	matrix of inverse Maxwell–Stefan coefficients, m^{-2} s
$[D]$	matrix of Fick diffusivities, $m^2 s^{-1}$
$D_{i,self}$	self-diffusivity, $m^2 s^{-1}$
$Đ_i$	Maxwell–Stefan diffusivity of species i in zeolite, $m^2 s^{-1}$
$Đ_i(0)$	zero-loading M–S diffusivity of species i in zeolite, $m^2 s^{-1}$
$Đ_{ii}$	self-exchange diffusivity, $m^2 s^{-1}$
$Đ_{ij}$	binary exchange diffusivity, $m^2 s^{-1}$
f_i	Reed–Ehrlich parameter, dimensionless
k_B	Boltzmann constant, 1.38×10^{-23} J molecule^{-1} K^{-1}
$L_{ij}k_BT$	(modified) Onsager coefficients, molecule $m^{-1} s^{-1}$
$\mathbf{N}_i$	molecular flux of species i, molecules $m^{-2} s^{-1}$
N_i	number of molecules of species i, molecules
p_i	partial pressure of species i, Pa
t	time, s
T	absolute temperature, K
V	volume, m^3
x_i	mole fraction of species i in mixture, dimensionless
z	coordination number, dimensionless

Greek letters

β_i	Reed–Ehrlich parameter, dimensionless
$[\Delta]$	matrix of Maxwell–Stefan diffusivities, $m^2 s^{-1}$
ε	Reed–Ehrlich parameter, dimensionless
$[\Gamma]$	matrix of thermodynamic factors, dimensionless
θ	total occupancy of mixture, dimensionless
θ_i	fractional occupancy of component i, dimensionless
Θ_i	molecular loading, molecules per unit cell
$\Theta_{i,sat}$	saturation loading, molecules per unit cell
μ_i	molar chemical potential, J molecule^{-1}
ρ	zeolite density, number of unit cells per m^3

Subscripts

sat	referring to saturation conditions
self	referring to self diffusivity
i, j	components in mixture

Vector and matrix notation

( )	vector
[ ]	square matrix

topologies such as AFI, AET and MOR [13,14]. It is well known that adsorption properties have a significant influence on diffusion behavior of molecules in zeolites and therefore we may expect that entropy effects would also affect the diffusion behavior in the one-dimensional channels of zeolites.

In the present study we use CBMC and MD simulations to investigate adsorption and diffusion characteristics of pure components, and mixtures, containing hexane isomers (*n*-hexane (nC6), 2-methylpentane (2MP) and 2,2-dimethylbutane (22DMB)) and butane isomers (*n*-butane (nC4) and iso-butane (iC4)) in MOR zeolite. The first objective of the present study is to underline the importance of entropy effects in both adsorption *and* diffusion in MOR. The second objective is to examine whether mixture diffusion behavior can be predicted using single component data alone. Such predictions have been shown to be possible, using the Maxwell–Stefan (M–S) formulation, for mixture diffusion in MFI, FAU and LTA in recent publications [15–17] but have not yet been demonstrated for one-dimensional zeolite channel topologies. The adsorption and diffusion characteristics in the one-dimensional MOR topology are compared with the corresponding behavior in three-dimensional intersecting channel topology of MFI and the three-dimensional cage topology of FAU.

2. CBMC and MD simulations

CBMC and MD simulations have been carried out for hexane and butane isomers, and their mixtures, in MOR (all silica zeolite). MOR consists of 12-ring (7.0 Å × 6.5 Å), with 8-ring (5.7Å × 2.6 Å) side-pockets, running along the *z*-direction (see Fig. 1); detailed crystallographic data are available elsewhere [18]. For comparison purposes, analogous simulations were also carried out for MFI (all silica) and FAU (96 Si, 96 Al) topologies. For both adsorption and diffusion simulations we use the united atom model. We consider the CH_x groups as single, chargeless interaction centers with their own effective potentials. The beads in the chain are connected by harmonic bonding potentials. A harmonic cosine bending potential models the bond bending between three neighboring beads, a Ryckaert–Bellemans potential controls the torsion angle. The beads in a

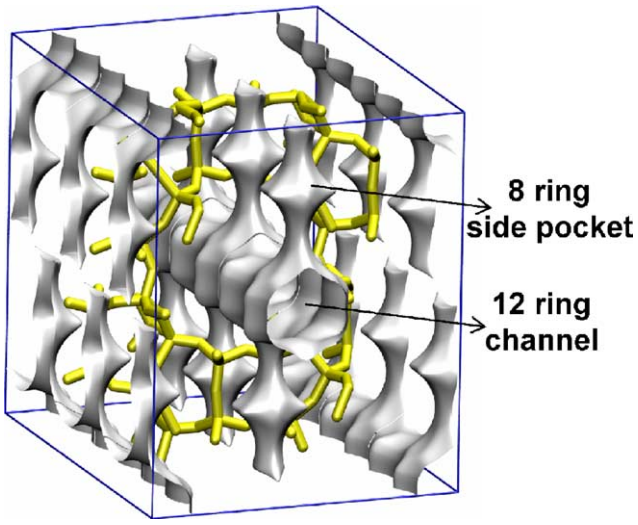

Fig. 1. Topology of MOR. The energy landscape diagram is obtained using a cut-off potential for CH2 of 20 kJ/mol.

chain separated by more than three bonds interact with each other through a Lennard-Jones potential. The Lennard-Jones potentials are shifted and cut at 12 Å. Pure component adsorption isotherms for alkanes were determined using configurational-bias Monte Carlo (CBMC) simulations. The CBMC simulation details, along with the force fields have been given in detail in other publications [19].

Diffusion in a system of N molecules is simulated using Newton's equations of motion until the system properties, on average, no longer change in time. The Verlet algorithm is used for time integration. The energy drift of the entire system is monitored to ensure that the time steps taken were not too large. A time step of 1 fs was used in all simulations. N molecules are inserted into the framework at random positions as long as no overlaps occur with the framework or other particles, and as long as the positions are accessible from the main cages and channels. During the initializing period we perform an NVT MC simulation to rapidly achieve an equilibrium molecular arrangement. After the initialization step, we assign velocities to the pseudo-atoms from the Maxwell–Boltzmann distribution at the desired average temperature. The total momentum of the system is set to zero. Next, we equilibrate the system further by performing a NVT MD simulation using the Nosé–Hoover thermostat. When the equilibration is completed, the production run starts. For every cycle, the statistics for determining the mean square displacements (MSDs) are updated. The MSDs are determined for time intervals ranging from 2 fs to 1 ns. In order to do this, an order-N algorithm, as detailed in Chapter 4 of Frenkel and Smit [20] is implemented.

The simulation boxes used for the CBMC and MD simulations are specified in Table 1; for MOR a higher number of unit cells in the z-direction were used in the MD simulations than for CBMC simulations in order to yield sufficiently good statistical data on the MSDs to allow accurate determination of the diffusivities.

Table 1
Simulation box dimensions as used in the CBMC and MD simulations

Zeolite	Number of unit cells	Cell dimensions
MOR (CBMC)	$2\times2\times4$	36.6 Å × 41.0 Å × 30.0 Å
MOR (MD)	$2\times2\times8$	36.6 Å × 41.0 Å × 60.0 Å
MFI (both CBMC and MD)	$2\times2\times2$	40.04 Å × 39.8 Å × 26.77 Å
FAU (both CBMC and MD)	$1\times1\times1$	25.03 Å × 25.03 Å × 25.03 Å

In the earlier publications of Sanborn and Snurr [21] and Skoulidas et al. [22], the Onsager matrix $[L]$, defined by $(\mathbf{N}) = -[L](\nabla\mu)$ were determined from the MSDs using linear response theory. From the viewpoint of determination of the M–S diffusivities, we find it much more convenient to define a matrix $[\Delta]$:

$$\mathbf{N}_i = -\frac{\rho}{k_B T}\Theta_i \sum_{j=1}^{n} \Delta_{ij}\nabla\mu_j, \quad i = 1,2,\ldots,n, \tag{1}$$

and determine the elements of this matrix from

$$\Delta_{ij} = \frac{1}{2N_i}\lim_{\Delta t\to\infty}\frac{1}{\Delta t}\left\langle\left(\sum_{l=1}^{N_i}\left(\mathbf{r}_{l,i}(t+\Delta t)-\mathbf{r}_{l,i}(t)\right)\right)\cdot\left(\sum_{k=1}^{N_j}\left(\mathbf{r}_{k,j}(t+\Delta t)-\mathbf{r}_{k,j}(t)\right)\right)\right\rangle. \tag{2}$$

In Eq. (2) N_i and N_j represent the number of molecules of species i and j, respectively, and $\mathbf{r}_{l,i}(t)$ is the position of molecule l of species i at any time t. From the definition $\Theta_i = N_i/\rho V$, where V is the volume of the simulation box, we see that $\rho\Theta_i\Delta_{ij} = L_{ij}k_B T$ and therefore the Onsager Reciprocal Relations $L_{ij} = L_{ji}$ lead to

$$\Theta_i\Delta_{ij} = \Theta_j\Delta_{ji}. \tag{3}$$

Eq. (2) applies to each of the three coordinate directions. For MOR, the subject of interest in this paper, only the z-direction yields non-zero diffusivities and these are reported here. For MFI and FAU, the Δ_{ij} reported are the orientation averaged ones, i.e., $\Delta_{ij} = (\Delta_{ij,x} + \Delta_{ij,y} + \Delta_{ij,z})/3$. Eq. (1) can be re-written as

$$(\mathbf{N}) = -\rho[\Delta][\Gamma](\nabla\Theta), \tag{4}$$

and therefore the matrix of Fick diffusivities, $[D]$ required for the solution of practical diffusion problems, is the product of $[\Delta]$ and the matrix of thermodynamic correction factors $[\Gamma]$:

$$[D] = [\Delta][\Gamma], \tag{5}$$

The elements Γ_{ij} of the matrix of thermodynamic factors can be calculated from knowledge of the multicomponent sorption isotherms [15,23]:

$$\frac{\Theta_i}{k_B T}\nabla\mu_i \equiv \sum_{j=1}^{n} \Gamma_{ij}\nabla\Theta_j,$$
$$\Gamma_{ij} = \frac{\Theta_i}{\Theta_j}\frac{\partial \ln p_i}{\partial \ln \Theta_j}, \quad i,j = 1,\ldots n, \tag{6}$$

where p_i represents the partial pressure (or, more strictly, the fugacity) of component i in the bulk fluid phase. For single component diffusion, $n = 1$, Δ_{11} can be identified with the M–S, or "corrected" diffusivity $Đ_1$, and the Fick diffusivity D_1 is given by

$$D_1 = Đ_1\Gamma, \quad \Gamma \equiv \frac{\partial \ln p}{\partial \ln \Theta}. \tag{7}$$

The self-diffusivities, $D_{i,\mathrm{self}}$, were computed by analyzing the mean square displacement of each component in the usual manner

$$D_{i,\mathrm{self}} = \frac{1}{2N_i}\lim_{\Delta t\to\infty}\frac{1}{\Delta t}\left\langle\left(\sum_{l=1}^{N_i}(\mathbf{r}_{l,i}(t+\Delta t) - \mathbf{r}_{l,i}(t))^2\right)\right\rangle. \tag{8}$$

Eq. (8) applies for each of the three coordinate directions. For MOR only the z-direction yields non-zero diffusivity values. For MFI and FAU, the orientation averaged values are reported in this paper.

The MD simulation data on Δ_{ij} and $D_{i,\mathrm{self}}$, at a specified loading, reported in this paper are averaged values from multiple simulations. The standard deviation of the individual simulations from the mean values were usually less than 5% of the mean values.

3. Simulation results and discussion

Let us first consider adsorption of the isomers nC6, 2MP and 22DMB in MOR at 433 K. CBMC simulations of the sorption isotherms are presented in Fig. 2a. The isotherms conform very closely to the dual site Langmuir isotherm

$$\Theta(p) \equiv \Theta_A + \Theta_B,$$
$$\Theta_A = \frac{\Theta_{\mathrm{sat,A}} b_A p}{1 + b_A p}, \quad \Theta_B = \frac{\Theta_{\mathrm{sat,B}} b_B p}{1 + b_B p}, \tag{9}$$

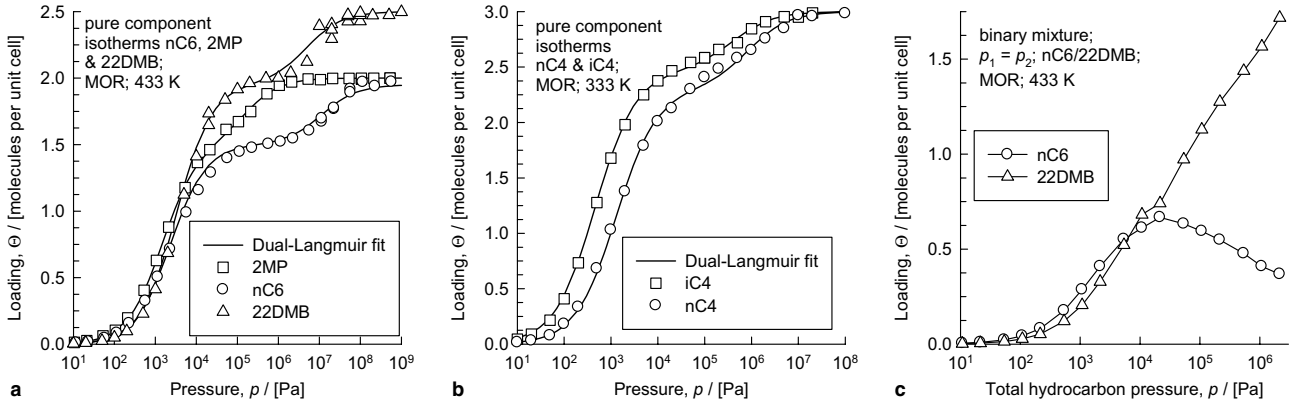

Fig. 2. (a) CBMC simulations (open symbols) of the sorption isotherms for (a) pure hexane isomers (nC6, 2MP, 22DMB; $T = 433$ K), and (b) butane isomers (nC4, iC4; $T = 333$ K) in MOR. The continuous solid lines in represent the dual-site Langmuir fits of the isotherms with the parameter values specified in Table 2. (c) CBMC simulations for binary mixture nC6(1)/22DMB(2), with $p_1 = p_2$, in MOR at $T = 433$ K.

Table 2
Dual-site Langmuir parameters for alkanes in MOR, FAU and MFI

Zeolite	Molecule	Temperature (K)	Dual-site Langmuir parameters			
			b_A	$\Theta_{\mathrm{sat,A}}$	b_B	$\Theta_{\mathrm{sat,B}}$
MOR	nC6	433	4.27×10^{-4}	1.5	8.78×10^{-8}	0.45
MOR	2MP	433	6.77×10^{-4}	1.5	6.34×10^{-6}	0.5
MOR	22DMB	433	3.06×10^{-4}	1.96	2.05×10^{-7}	0.54
MOR	nC4	333	7.76×10^{-4}	2.3	1.20×10^{-6}	0.7
MOR	iC4	333	2.17×10^{-3}	2.47	2.50×10^{-6}	0.53
FAU	nC6	433	1.52×10^{-5}	26	5.58×10^{-9}	6
FAU	2MP	433	2.17×10^{-5}	25	6.61×10^{-9}	7
MFI	nC6	433	8.35×10^{-4}	4	1.35×10^{-5}	4
MFI	2MP	433	9.43×10^{-4}	4	8.01×10^{-9}	4
MFI	22DMB	433	2.53×10^{-4}	4	–	–

The saturation capacity Θ_{sat} has the units of molecules per unit cell. The Langmuir parameters b_i, have the units of Pa^{-1}.

with fitted DSL model parameters as specified in Table 2. In eq. (9) b_A and b_B represent the DSL model parameters expressed in Pa^{-1} and the subscripts A and B refer to two sorption sites within the zeolite structure, with different sorption capacities and sorption strengths. The $\Theta_{sat,A}$ and $\Theta_{sat,B}$ represent the saturation capacities of sites A and B, respectively. The saturation capacities, $\Theta_{sat} = \Theta_{sat,A} + \Theta_{sat,B}$, of the hexane isomers increase with the degree of branching. This is due to the increased packing efficiency with increased degree of branching in one-dimensional channels, as has been explained in the published literature [14,24]. By examination of the snapshots of the location of the molecules within the MOR topology it is clear that the hexane isomers are only adsorbed within the 12-ring channels. Some representative snapshots showing the siting and conformation of the molecules along one of the 12-ring channels, 8 unit cells long, are seen in Fig. 3b–d for a pressure $p = 100$ kPa. Within the same channel length we find 5 nC6 molecules, 7 2MP molecules and 9 22DMB molecules. The higher loading with increased degree of branching is due to increased degree of compactness of the molecules. The more compact the molecule, the higher the packing efficiency within the one-dimensional channels. This point is emphasized further by determining the projected lengths of the molecules of the hexane isomers on the z-axis for $p = 100$ kPa; the data on the distribution of molecular lengths are shown in Fig. 4a. The projected lengths are obtained by monitoring the positions of each of the pseudo-atoms in the alkane molecules and determining the maximum span of the molecule by projecting the positions of the pseudo-atoms along the direction of the 12-ring channels. The mean length of the hexane isomers are 5.2 Å, 4.3 Å and 3 Å for nC6, 2MP and 22DMB, respectively. This data also explains why the saturation capacity for 22DMB is significantly higher ($\Theta_{sat} = 2.5$), compared to that for 2MP ($\Theta_{sat} = 2.0$) and nC6 ($\Theta_{sat} = 1.95$).

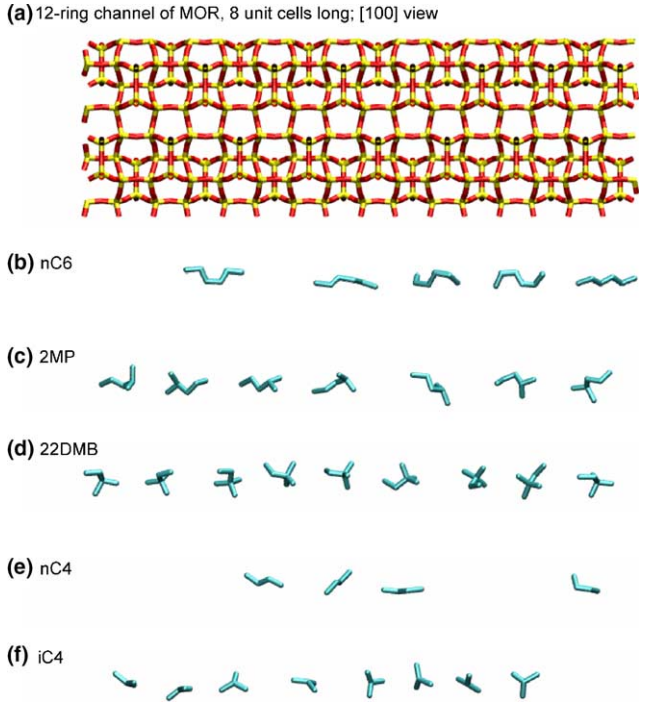

Fig. 3. (a) One 12-ring channel of MOR, [1 0 0] view. Snapshots of the conformation and siting of (b–d) hexane and (e,f) butane isomers along the 12-ring channel of MOR.

A similar picture emerges from the CBMC simulations for butane isomers in MOR at 333 K. The pure component sorption isotherms are shown in Fig. 2b. The branched isomer iC4 shows a higher loading Θ for all pressures $p < 10{,}000$ kPa. Snapshots of the conformation and siting along one 12-ring channel of MOR are shown in Fig. 3e and f, for pressure $p = 1$ kPa. We note that at this pressure 8 iC4 molecules can be accommodated whereas only 4 nC4 molecules are found. The corresponding molecular length distribution data are presented in Fig. 4b. The mean length of the

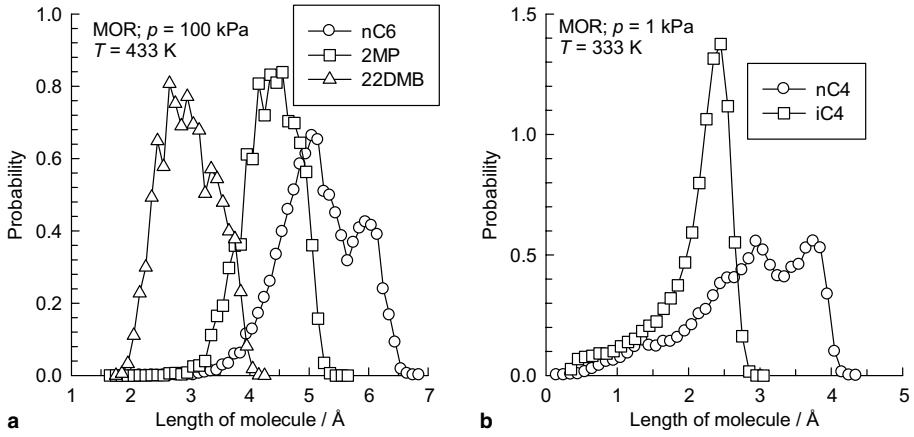

Fig. 4. Distribution of lengths of (a) hexane isomers ($p = 100$ kPa, $T = 433$ K), and (b) butane isomers ($p = 1$ kPa, $T = 333$ K) along the z-direction of MOR obtained from CBMC simulations.

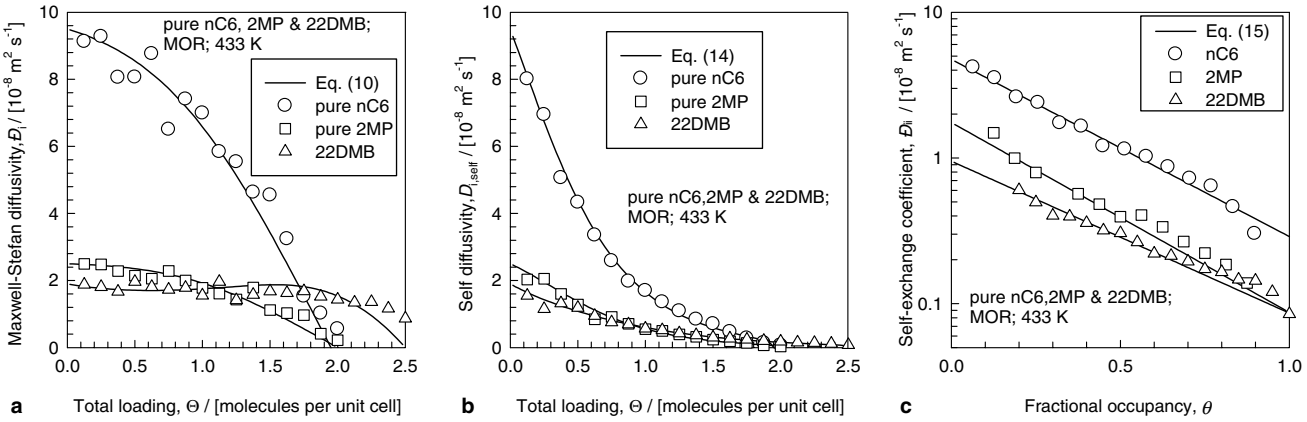

Fig. 5. (a) Maxwell–Stefan diffusivities $Đ_i$, (b) self-diffusivities $D_{i,\text{self}}$, and (c) self-exchange coefficients $Đ_{ii}$ of hexane isomers in MOR at 433 K, as a function of the molecular loading Θ, or occupancy θ, determined by MD simulations (open symbols). The continuous solid lines in (a) represent the calculations using Eqs. (10) and (11), respectively, using the parameters specified in Table 3. The continuous lines in (b) and (c) are drawn using Eqs. (14) and (15) using the parameters specified in Table 3.

butane isomers are approximately 2.9 Å and 2.1 Å for nC4 and iC4, respectively. We also note that a significant proportion of the data on molecular lengths show nearly zero lengths, implying that the molecular conformations are such that molecules are stretched in a direction orthogonal to the axis of the channels.

Entropy effects have a pronounced effect on adsorption in mixtures. In order to illustrate this we carried out CBMC simulations for the binary mixture nC6/22DMB in MOR at $T = 433$ K keeping the partial pressures of the two isomers the same, i.e., $p_1 = p_2$ at low pressures, $p = p_1 + p_2 < 5$ kPa, nC6 adsorbs more strongly than 22DMB, but for $p > 5$ kPa, 22DMB adsorbs more strongly than nC6; see Fig. 2c. This reversal of selectivity in favor of 22DMB is caused due to its higher packing efficiency at high loadings.

We now examine the influence of packing efficiency effects on diffusion of hexane and butane isomers in MOR. The MD simulation results for the M–S diffusivity $Đ_i$, self-diffusivities $D_{i,\text{self}}$, and self-exchange coefficients $Đ_{ii}$ of nC6, 2MP and 22DMB in MOR at 433 K are shown by the open symbols in Fig. 5a–c. Note that the reported diffusivities are based on diffusion in the z-direction alone. Typical MSD data, monitored in the z-direction of MOR, for nC6 and 22DMB at a loading $\Theta = 0.5$ are shown in Fig. 6. We note that the MSDs vary linearly with t and not $t^{1/2}$; this precludes single file diffusion behavior. This conclusions is also in agreement with that drawn by Schuring et al. [11] on the basis of MD simulations. Both $Đ_i$ and $D_{i,\text{self}}$ tend to approach near-zero values at saturation loadings $\Theta = \Theta_{\text{sat}}$. For loadings $\Theta < 1$, the hierarchy of the M–S diffusivity values is dictated by the degree of branching with the "slimmer" nC6 molecule having the highest diffusivity and the most compact 22DMB molecule having the lowest diffusivity. Since the saturation capacities increase with the degree of branching, an interesting reversal takes place

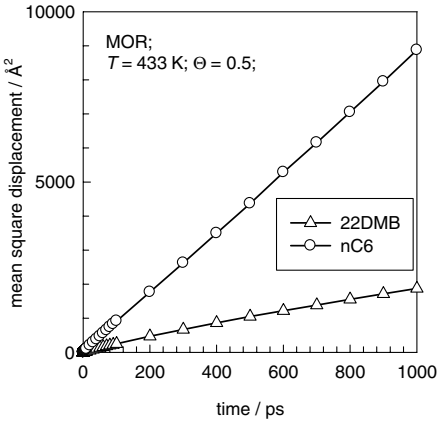

Fig. 6. Typical MSD data for nC6 and 22DMB in MOR at 433 K at a loading $\Theta = 0.5$.

in the hierarchy of M–S diffusivities. 22DMB diffuses faster than 2MP for $\Theta > 1$, and faster than both nC6 and 2MP for $\Theta > 1.8$. This highlights the influence of packing efficiency effects at higher loadings.

We also note that the loading dependence of $Đ_i$ for the di-branched isomer 22DMB is qualitatively different to that of the other isomers nC6 and 2MP. For nC6 and 2MP, the $Đ_i$ decreases almost linearly with loading to zero values at saturation $\Theta = \Theta_{\text{sat}}$. For 22DMB, on the other hand, the $Đ_i$ remains nearly constant for a range of loading until saturation values are approached and only then does $Đ_i$ appear to reduce to zero. From the work of Tunca and Ford [25] and Beerdsen et al. [26] it can be concluded that the loading dependence is dictated by the influence of the loading on the energy barrier for diffusion. The model due to Reed and Ehrlich [27,28], developed originally for diffusion on a two-dimensional square lattice of sites, provides a simple approach to quantification of the loading dependence of the M–S diffusivity $Đ_i$. In the Reed–Ehrlich model, the

presence of neighboring molecules on a lattice is assumed to influence the jump frequencies of species i by a factor $f_i = \exp\left(\frac{\delta E_i}{RT}\right)$, where δE_i represents the reduction in the energy barrier for diffusion. This model leads to the following expression for the M–S diffusivity as a function of the fractional occupancy:

$$Đ_i = Đ_i(0)\frac{(1+\varepsilon_i)^{z-1}}{(1+\varepsilon_i/f_i)^z}, \tag{10}$$

where z is the coordination number, representing the maximum number of nearest neighbors. In the case of one-dimensional transport along the 12-ring channels of MOR we may take $z = 2$. The other parameters are defined as (see [28] for more detailed discussions and derivations)

$$\varepsilon_i = \frac{(\beta - 1 + 2\theta_i)f_i}{2(1-\theta_i)},$$
$$\beta = \sqrt{1 - 4\theta_i(1-\theta_i)(1-1/f_i)}, \tag{11}$$

where the fractional occupancies θ_i defined by

$$\theta_i \equiv \Theta_i/\Theta_{i,\mathrm{sat}}, \quad i = 1, 2, \ldots, n. \tag{12}$$

In the limiting case where there are no interactions between neighboring molecules, i.e., $\delta E_i = 0$, we get $f_i = 1$, $\beta_i = 1$, $\varepsilon_i = \theta_i/(1-\theta_i)$ and Eq. (10) reduces to yield

$$Đ_i = Đ_i(0)(1-0_i) = Đ_i(0)\left(1 - \frac{\Theta_i}{\Theta_{i,\mathrm{sat}}}\right). \tag{13}$$

The fitted values of f are specified in Table 3. The continuous solid lines in Fig. 5a are drawn using these parameter values in Eqs. (10) and (11). The Reed–Ehrlich model does a good job of describing the loading dependence of all three hexane isomers.

From the data on the M–S and self-diffusivities, the self-exchange coefficients $Đ_{ii}$ can be calculated

$$Đ_{ii} = \frac{\theta_i}{\frac{1}{D_{i,\mathrm{self}}} - \frac{1}{Đ_i}}, \quad D_{i,\mathrm{self}} = \frac{1}{\frac{1}{Đ_i} + \frac{\theta_i}{Đ_{ii}}}. \tag{14}$$

In the work of Skoulidas et al. [15,29] the self-exchange coefficient was fitted in the form $\frac{Đ_{ii}}{Đ_i} = a_i \exp(-b_i\theta_i)$. For the molecule-zeolite systems considered in this paper the M–S diffusivity $Đ_{ii}$ reduces to zero at saturation loading (see Fig. 5a) and, consequently, the self-exchange coefficient $Đ_{ii}$ is also predicted to reduce to zero by their correlation. However the simulated data show that $Đ_{ii}$ do not reduce to zero; rather they decay exponentially with θ and have a small but finite value at $\theta = 1$; this is shown for example in Fig. 5c. For this reason we chose to correlate the $Đ_{ii}$ in the following manner:

$$\frac{Đ_{ii}}{Đ_i(0)} = a_i \exp(-b_i\theta_i), \tag{15}$$

with the values of the a_i and b_i as given in Table 3. The self-exchange coefficients are essential in the description of mixture diffusion as they describe correlation effects [15,17]. It is worth mentioning here that for single-file diffusion Eq. (14) is not well defined [30].

The MD simulations of the elements of the matrix $[Đ]$ for equimolar mixtures of (a) nC6/2MP, (b) nC6/22DMB, (c) 2MP/22DMB and (d) nC6/2MP/22DMB are shown by open symbols in Fig. 7. For the ternary mixture only the diagonal elements $Đ_{ii}$ are shown. For the three binary mixtures we note that the cross-coefficient $Đ_{12}$ has values comparable to that of the diagonal elements $Đ_{11}$ and $Đ_{22}$, for loadings $\Theta > 1$. This suggests that correlation effects are particularly significant for diffusion within the 12-ring channels of MOR.

Let us now attempt to predict the elements of the matrix $[Đ]$ using the M–S diffusion equations

$$-\rho\frac{\Theta_i}{k_B T}\nabla\mu_i = \sum_{\substack{j=1\\ j\neq i}}^{n}\frac{\Theta_j \mathbf{N}_i - \Theta_i \mathbf{N}_j}{\Theta_{j,\mathrm{sat}} Đ_{ij}} + \frac{\mathbf{N}_i}{\Theta_{i,\mathrm{sat}} Đ_i}, \quad i = 1, \ldots, n, \tag{16}$$

where n is the total number of diffusing species and k_B is the Boltzmann constant. Eq. (16) *defines* two types of

Table 3
Pure component diffusion data for alkanes in MOR and FAU

Component and zeolite	Saturation capacity, $\Theta_{i,\mathrm{sat}}$	$Đ_i(0)$	Parameters describing self-exchange, defined by Eq. (14)		Reed–Ehrlich model parameters in Eqs. (10) and (11)	
			a_i	b_i	z	f
nC6/MOR/433 K	1.95	9.5	0.5	2.8	2	1.6
2MP/MOR/433 K	2.0	2.5	0.7	3.0	2	1.8
22DMB/MOR/433 K	2.5	1.9	0.5	2.4	2	$1.0\exp(1.8\theta)$
nC4/MOR/333 K	3	6.7	0.25	2.8	2	1.6
iC4/MOR/333 K	3	3.5	0.25	1.55	2	$1.5\exp(1.3\theta)$
nC6/FAU/433 K	32	1.05	3.5	3.0	–	1
2MP/FAU/433 K	32	0.87	2.5	3.0	–	1

The $Đ_i(0)$ values have the units 10^{-8} m^2 s^{-1}. The saturation capacity Θ_{sat} has the units of molecules per unit cell.

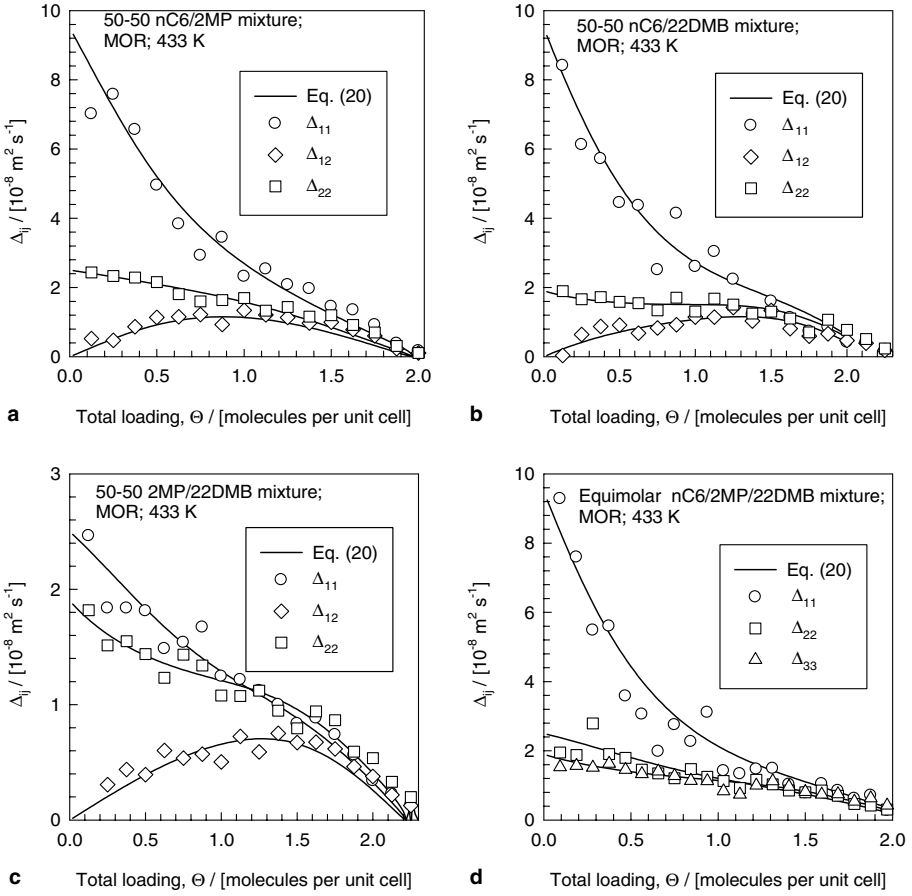

Fig. 7. MD simulation data (open symbols) of Δ_{ij} for equimolar mixtures (a) nC6/2MP, (b) nC6/22DMB, (c) 2MP/22DMB and (d) nC6/2MP/22DMB in MOR at 433 K. The continuous solid lines are calculations following Eq. (20), with parameter values are given in Table 3.

M–S diffusivities: $Đ_i$ and $Đ_{ij}$. The $Đ_i$ are the same as the pure component diffusivities provided these are determined at the same occupancy $\theta = \sum_{i=1}^{n} \Theta_i/\Theta_{i,\mathrm{sat}}$; this has been verified for binary, ternary and quaternary alkane mixtures in FAU, MFI and LTA [17]. The binary exchange coefficients $Đ_{ij}$ reflect *correlation* effects in mixture diffusion [15,17]. For mixture diffusion, the $Đ_{ij}$ tends to slow down the more mobile species and speed up the relatively sluggish ones. A lower value of the exchange coefficient $Đ_{ij}$ implies a *stronger* correlation effect. When $Đ_{ij} \to \infty$, correlation effects vanish. For n-component mixtures, a logarithmic interpolation formula has been suggested [17]:

$$\Theta_{j,\mathrm{sat}} Đ_{ij} = [\Theta_{j,\mathrm{sat}} Đ_{ii}]^{\Theta_i/(\Theta_i+\Theta_j)} [\Theta_{i,\mathrm{sat}} Đ_{jj}]^{\Theta_j/(\Theta_i+\Theta_j)}, \quad i,j = 1,2,\ldots,n, \tag{17}$$

for estimating the binary exchange parameter $Đ_{ij}$ from information on the pure component *self*-exchange coefficients $Đ_{ii}$ and $Đ_{jj}$. Eq. (17) has been validated for alkane mixtures in FAU, MFI and LTA [16,17]. Defining an n-dimensional square matrix $[B]$ with elements

$$B_{ii} = \frac{1}{Đ_i} + \sum_{\substack{j=1 \\ j\neq i}}^{n} \frac{\Theta_j}{Đ_{ij}}, \quad B_{ij} = -\frac{\Theta_{i,\mathrm{sat}}}{\Theta_{j,\mathrm{sat}}} \frac{\Theta_i}{Đ_{ij}}, \quad i,j = 1,2\ldots,n, \tag{18}$$

allows us to recast Eq. (16) into n-dimensional matrix notation as

$$(\mathbf{N}) = -\rho[B]^{-1}[\Gamma](\nabla\Theta). \tag{19}$$

Comparing Eqs. (4) and (19) we obtain the following relation that allows the prediction of the elements of $[Đ]$ from *pure* component data on $Đ_i$ and $Đ_{ii}$:

$$[Đ] = [B]^{-1}. \tag{20}$$

In these predictions the occupancy $\theta = \sum_{i=1}^{n} \Theta_i/\Theta_{i,\mathrm{sat}}$ in the *mixture* is used in Eqs. (10) and (15). The calculations using Eq. (20), with parameter values given in Table 3, are shown by the continuous solid lines in Fig. 7. We note that the predictions are good for all three binary mixtures and the ternary mixture, over the entire range of loadings.

Let us now consider diffusion of butane isomers. The pure component diffusivity data for nC4 and iC4 in

MOR at 333 K are shown in Fig. 8a–c; the diffusion parameters are listed in Table 3. For loadings $\Theta < 2$, the hierarchy of the M–S diffusivity values is dictated by the degree of branching with the "slimmer" nC4 molecule having the highest diffusivity and the more compact iC4 molecule having the lower diffusivity. Packing efficiency considerations cause a reversal to take place in the hierarchy of M–S diffusivities and iC4 diffuses faster than nC4 for $\Theta > 2$. The loading dependence of the branched isomer is also quite different from the linear one, as is evidenced by the values of the Reed–Ehrlich parameter f, listed in Table 3. As in the case for the hexane isomers, the predictions of the matrix $[\Delta]$ for diffusion in the equimolar binary nC4/iC4 binary from *pure* component data on $Đ_i$ and $Đ_{ii}$ are good for the entire range of molecular loadings; see Fig. 8d. Another point to note in Fig. 8d is that the cross-coefficient Δ_{12} has values comparable to that of the diagonal elements Δ_{11} and Δ_{22}, for loadings $\Theta > 1.5$, stressing the importance of correlation effects in mixture diffusion, especially at high loadings. Apparently, these correlation effects are well predicted by the binary exchange coefficients $Đ_{ij}$ and use of the interpolation formula (17).

In order to stress the differences in the adsorption and diffusion characteristics of MOR and other zeolites, we also carried out CBMC and MD simulations of hexane isomers in FAU and MFI at 433 K; the data are presented in Figs. 9 and 10. The FAU topology consists of cages separated from one another by large windows. The pure component sorption isotherms of nC6 and 2MP are nearly the same and there is no strong preference for adsorption of either isomer; see Fig. 9a. Put another way, entropy effects play no role for adsorption of hexane isomers in FAU. The pure component diffusivities of the hexane isomers are close to one another (see Fig. 9b and c). The loading dependence of the M–S diffusivity follows Eq. (13), suggesting that there is no influence of the molecular loading on the activation energy for diffusion, i.e., $\delta E_i = 0$, $f_i = 1$. The elements of the matrix $[\Delta]$ for binary mixture diffusion can be well predicted from the pure component adsorption and diffusion data, as is evidenced by comparisons of the

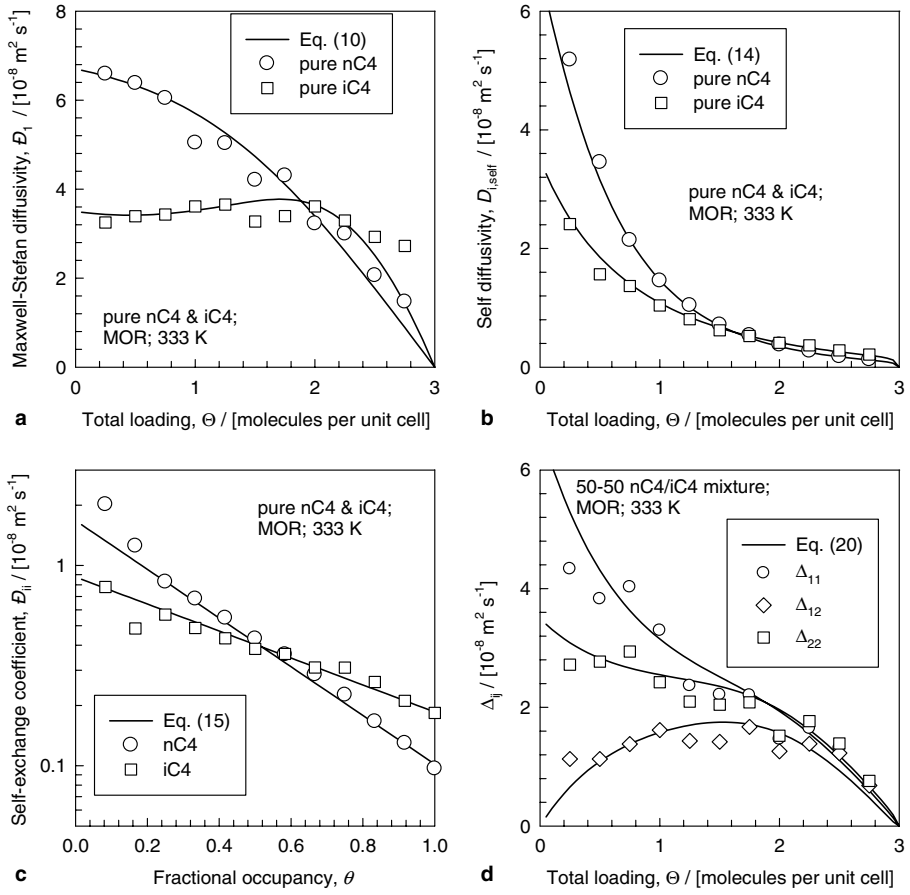

Fig. 8. (a) Maxwell–Stefan diffusivities $Đ_i$, (b) self-diffusivities $D_{i,\text{self}}$ and (c) self-exchange coefficients $Đ_{ii}$ of butane isomers (nC4 and iC4) in MOR at 333 K, as a function of the molecular loading Θ, or occupancy θ, determined by MD simulations (open symbols). The continuous solid lines in (a) represent the calculations using Eqs. (10) and (11), respectively, using the parameters specified in Table 3. The continuous lines in (b) and (c) are drawn using Eqs. (14) and (15) using the parameters specified in Table 3. (d) MD simulation data (open symbols) of Δ_{ij} for equimolar binary mixture nC4/iC4 in MOR at 333 K. The continuous solid lines are calculations following Eq. (20), with parameter values are given in Table 3.

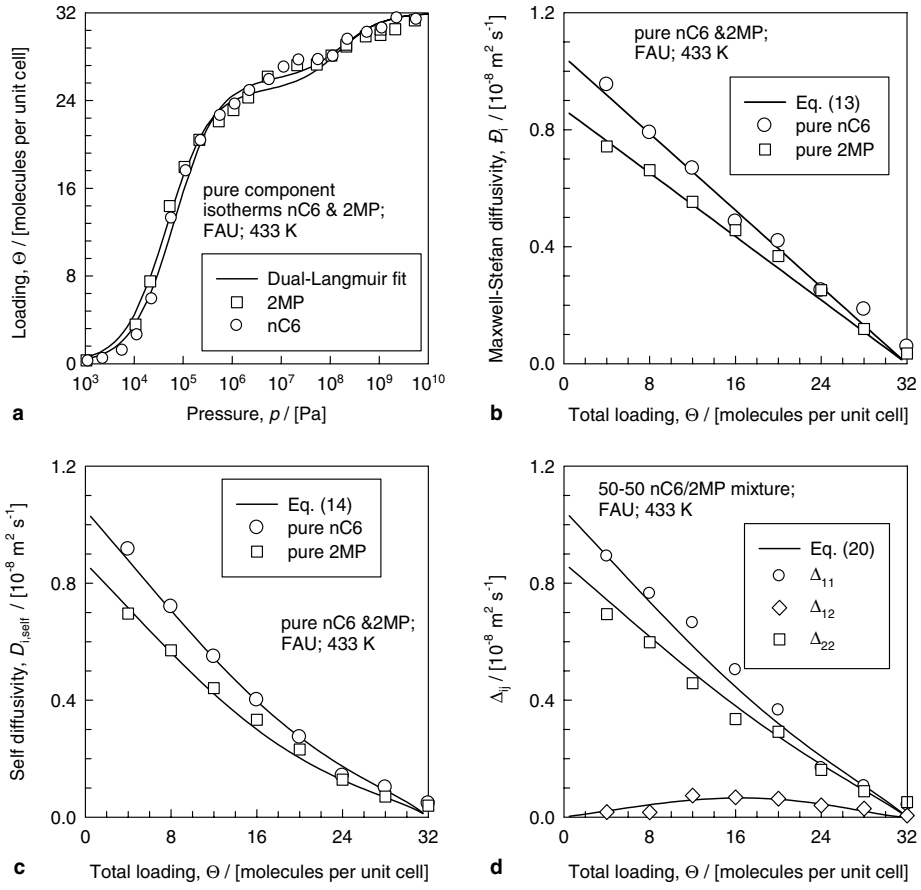

Fig. 9. (a) CBMC simulations (open symbols) of the sorption isotherms for (a) hexane isomers (nC6, 2MP) in FAU at 433 K. The continuous solid lines represent the dual-site Langmuir fits of the isotherms with the parameter values specified in Table 2. (b) Maxwell–Stefan diffusivities $Đ_i$ and (c) self-diffusivities $D_{i,\mathrm{self}}$ of pure hexane isomers (nC6, 2MP) in FAU at 433 K, as a function of the molecular loading Θ, determined by MD simulations (open symbols). The continuous solid lines in (b) represent the calculations using Eq. (13), respectively, using the parameters specified in Table 3. The continuous lines in (c) are drawn using Eqs. (14) and (15) using the parameters specified in Table 3. (d) MD simulation data (open symbols) of Δ_{ij} for equimolar binary mixture nC6/2MP in FAU at 433 K. The continuous solid lines are calculations following Eq. (20), with parameter values are given in Table 3.

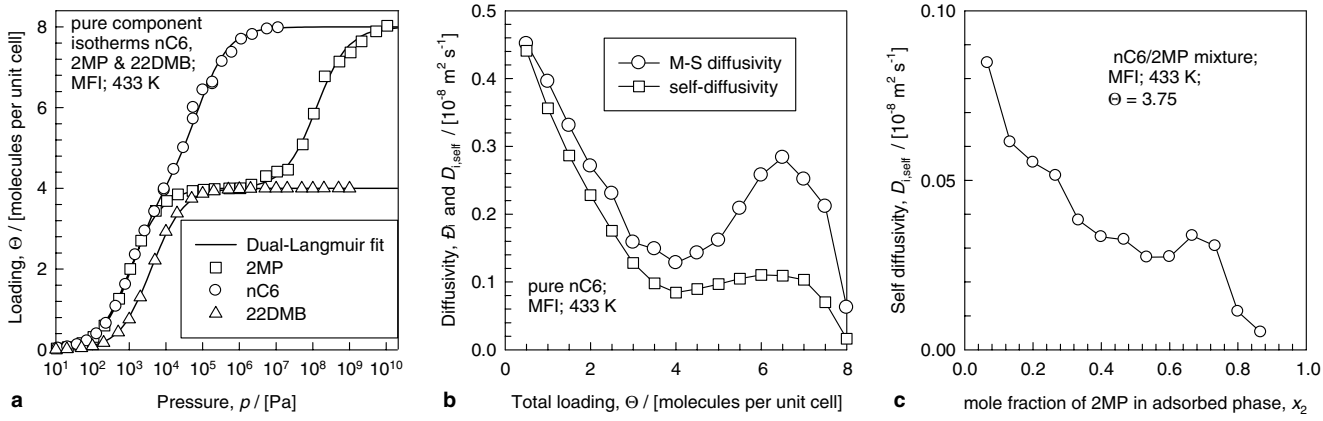

Fig. 10. (a) CBMC simulations (open symbols) of the sorption isotherms for (a) hexane isomers (nC6, 2MP, 22DMB) in MFI at 433 K. The continuous solid lines represent the dual-site Langmuir fits of the isotherms with the parameter values specified in Table 2. (b) Maxwell–Stefan diffusivities $Đ_i$ and self-diffusivities $D_{i,\mathrm{self}}$ of pure hexane isomers in MFI at 433 K, as a function of the molecular loading Θ, determined by MD simulations (open symbols). (c) MD simulation data (open symbols) of $D_{i,\mathrm{self}}$ for binary mixture nC6/2MP at a total loading $\Theta = 3.75$ in MFI at 433 K with varying proportions of the hexane isomers.

predictions (continuous solid lines) and MD simulations (open symbols) in Fig. 9d. Another point to note is that the cross-coefficient Δ_{12} has relatively small values compared to the diagonal elements Δ_{11} and Δ_{22}. This would suggest that correlation effects are rather weak in the FAU topology, in sharp contrast to MOR where correlation effects for diffusion in the one-dimensional channels are strong.

For adsorption of the hexane isomers within the intersecting channel structure of MFI, packing efficiency effects act in a manner opposite to that in MOR. The branched isomers 2MP and 22DMB are preferentially located at the intersections and at a loading $\Theta = 4$, all the intersection sites are occupied [14,24,31,32]. 2MP can locate in the channel interiors only when the pressures are increased substantially; this explains the strong inflection in the 2MP isotherm shown in Fig. 10a. The nC6 isotherm also exhibits a slight inflection at $\Theta = 4$; this is due to commensurate "freezing" [31,33]. The 22DMB molecule is so bulky that it cannot be located within the channel interiors and its saturation $\Theta_{sat} = 4$. The pure component M–S and self-diffusivities of nC6 are shown in Fig. 10b. The loading dependence of $Đ_i$ shows inflection behavior at $\Theta = 4$, corresponding to the isotherm inflection as has been explained in earlier publications [34–36]. Since the 2MP and 22DMB molecules are firmly ensconced at the intersection sites, their diffusivity values are too low to be monitored accurately using MD simulations. We carried out MD simulations for binary mixtures of nC6 and 2MP at a total loading $\Theta = 3.75$ and varying the proportion of the hexane isomers; these stimulations were performed in order to compare with the experimental data published by Schuring et al. [37] The MD results for $D_{i,self}$ of nC6 are shown as a function of the mole fraction of 2MP in the mixture in Fig. 10c. We note the strong decrease in the nC6 diffusivity as the proportion of 2MP increases. Snapshots of the siting of the nC6 and 2MP molecules are shown in Fig. 11 viewed (a) along [0 1 0] and (b) [0 0 1]. The 2MP molecules are only to be found at the intersections, whereas the nC6 molecules are located along both the straight channels and the zig-zag channels. The movement of nC6 molecules must proceed via the intersections, that act like traffic junctions. Since the practically immobile 2MP molecules occupy the intersections, the traffic of nC6 molecules is seriously impaired. The strong decline, that is about one order of magnitude, in the nC6 diffusivity due to the presence of 2MP has been verified experimentally by Schuring et al. [37].

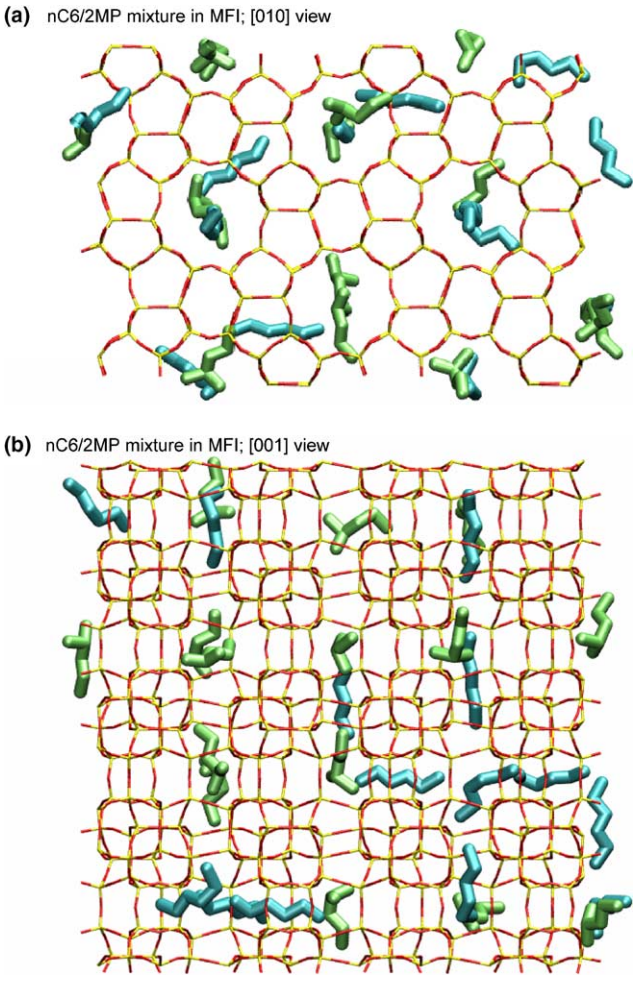

Fig. 11. (a) [0 1 0] and (b) [0 0 1] views of snapshots showing location of nC6 (1) and 2MP (2) molecules for binary mixture in MFI at $T = 433$ K and $p_1 = 3.3$ kPa, $p_2 = 3.3$ kPa.

4. Conclusions

In this paper we have used CBMC and MD simulations to investigate adsorption and diffusion of alkane isomers in MOR, FAU and MFI. The following major conclusions can be drawn from this work.

Adsorption and diffusion in MOR takes place exclusively within the 12-ring channels. The diffusion is unidimensional and no single file diffusion behavior could be detected for either hexane or butane isomers. From snapshots of the CBMC simulations we find that the molecules are aligned along the axis of the channels of MOR. The more compact branched isomers, with a smaller effective molecular length, have a higher packing efficiency within the channels. Consequently their adsorption strength, and capacity, is higher.

At low loadings the hierarchy of diffusivities is such that the slimmer linear isomer diffuses faster than the more compact branched ones. In all cases the $Đ_i \to 0$ as $\Theta \to \Theta_{sat}$. Packing entropy phenomena cause a reversal in the hierarchy of diffusivity values as saturation loadings are approached. Consequently at high Θ, 22DMB diffuses faster than nC6 and iC4 diffuses faster than nC4. This phenomenon of diffusivity reversal has never been reported earlier in the published literature.

The Reed–Ehrlich model provides an adequate continuum description of the loading dependence of $Đ_i$; the parameter f, needs to be fitted to the MD simulated data. There is hope, however, that this parameter f can be estimated using the transition state theory, as described in the work of Beerdsen et al. [26].

For diffusion in equimolar mixtures of hexane and butane isomers, the elements of the matrix $Δ_{ij}$ were determined for a range of molecular loadings within MOR. The cross-coefficient $Δ_{12}$ was found to be of the same order of magnitude as the diagonal elements at high loadings. This suggests strong correlation effects in mixture diffusion. The Maxwell–Stefan diffusion formulation has been shown to be capable of predicting $Δ_{ij}$ using only pure component diffusion data. For these predictions correlation effects embodied in the self-exchange coefficients $Đ_{ii}$ need to be properly described.

For FAU, it was found that the linear and branched isomer have nearly the same adsorption strength. The diffusivities of the pure components were also close to one another, and correlation effects, quantified by the cross-coefficients $Δ_{12}$ were found to be negligibly small. This result is expected; the large windows of FAU do not distinguish between linear and branched isomers.

For MFI, the entropy effects act in a manner opposite to that for MOR. The branched 2MP prefers to locate at the intersections, and has a negligibly small diffusivity compared to the linear nC6. For mixture diffusion, the presence of 2MP seriously hinders the diffusion of nC6, as has been found experimentally [37].

The work presented in this paper should provide guidelines for choosing the proper catalyst and adsorbent for alkane isomerization processes [24]. The adsorption and diffusion data presented here should also be useful in the design and optimization of such processes.

Acknowledgements

R.K. acknowledges two grants: *Programmasubsidie* and TOP subsidy from the Netherlands Foundation for Fundamental Research (NWO-CW) for the development of novel concepts in reactive separations technology and for intensification of reactors. We gratefully acknowledge D. Dubbeldam, S. Calero, T.J.H. Vlugt, E. Beerdsen and B. Smit for providing the CBMC and MD simulation codes. We acknowledge NWO/NCF for provision of high performance computing resources.

References

[1] S. Calero, M. Schenk, D. Dubbeldam, T.L.M. Maesen, B. Smit, The selectivity of *n*-hexane hydroconversion on MOR-, MAZ-, and FAU-type zeolites, J. Catal. 228 (2004) 121–129.

[2] T. Sano, S. Wakabayashi, Y. Oumi, T. Uozumi, Synthesis of large mordenite crystals in the presence of aliphatic alcohol, Micropor. Mesopor. Mater. 46 (2001) 67–74.

[3] B.O. Hincapie, L.J. Garces, Q.H. Zhang, A. Sacco, S.L. Suib, Synthesis of mordenite nanocrystals, Micropor. Mesopor. Mater. 67 (2004) 19–26.

[4] P.K. Bajpai, Synthesis of mordenite type zeolite, Zeolites 6 (1986) 2–8.

[5] T.C. Bowen, R.D. Noble, J.L. Falconer, Fundamentals and applications of pervaporation through zeolite membranes, J. Membr. Sci. 245 (2004) 1–33.

[6] M.W. Ackley, S.U. Rege, H. Saxena, Application of natural zeolites in the purification and separation of gases, Micropor. Mesopor. Mater. 61 (2003) 25–42.

[7] J.E. Gilbert, A. Mosset, Large crystals of mordenite and MFI zeolites, Mater. Res. Bull. 33 (1998) 997–1003.

[8] F.J.M.M. de Gauw, J. van Grondelle, R.A. van Santen, Effects of single-file diffusion on the kinetics of hydroisomerization catalyzed by Pt/H-mordenite, J. Catal. 204 (2001) 53–63.

[9] S. van Donk, A. Broersma, O.L.J. Gijzeman, J.A. van Bokhoven, J.H. Bitter, K.P. de Jong, Combined diffusion, adsorption, and reaction studies of *n*-hexane hydroisomerization over Pt/H-mordenite in an oscillating microbalance, J. Catal. 204 (2001) 272–280.

[10] L.A. Clark, A. Gupta, R.Q. Snurr, Siting and segregation effects of simple molecules in zeolites MFI, MOR, and BOG, J. Phys. Chem. B 102 (1998) 6720–6731.

[11] D. Schuring, A.P.J. Jansen, R.A. van Santen, Concentration and chainlength dependence of the diffusivity of alkanes in zeolites studied with MD simulations, J. Phys. Chem. B 104 (2000) 941–948.

[12] L. Domokos, L. Lefferts, K. Seshan, J.A. Lercher, Applied molecular simulations over FER-, TON-, and AEL-type zeolites, J. Catal. 203 (2002) 351–361.

[13] M. Schenk, S. Calero, T.L.M. Maesen, L.L. van Benthem, M.G. Verbeek, B. Smit, Understanding zeolite catalysis: inverse shape selectivity revised, Angew. Chem.-Int. Edit. 41 (2002) 2500–2502.

[14] R. Krishna, B. Smit, S. Calero, Entropy effects during sorption of alkanes in zeolites, Chem. Soc. Rev. 31 (2002) 185–194.

[15] A.I. Skoulidas, D.S. Sholl, R. Krishna, Correlation effects in diffusion of CH4/CF4 mixtures in MFI zeolite. A study linking MD simulations with the Maxwell–Stefan formulation, Langmuir 19 (2003) 7977–7988.

[16] S. Chempath, R. Krishna, R.Q. Snurr, Nonequilibrium MD simulations of diffusion of binary mixtures containing short *n*-alkanes in faujasite, J. Phys. Chem. B 108 (2004) 13481–13491.

[17] R. Krishna, J.M. van Baten, Diffusion of alkane mixtures in zeolites. Validating the Maxwell–Stefan formulation using MD simulations, J. Phys. Chem. B 109 (2005) 6386–6396.

[18] C. Baerlocher, L.B. McCusker, Database of zeolite structures, <http://www.iza-structure.org/databases/>, accessed 12 October 2004.

[19] D. Dubbeldam, S. Calero, T.J.H. Vlugt, R. Krishna, T.L.M. Maesen, B. Smit, United atom forcefield for alkanes in nanoporous materials, J. Phys. Chem. B 108 (2004) 12301–12313.

[20] D. Frenkel, B. Smit, Understanding Molecular Simulations: from Algorithms to Applications, second ed., Academic Press, San Diego, 2002.

[21] M.J. Sanborn, R.Q. Snurr, Diffusion of binary mixtures of CF4 and *n*-alkanes in faujasite, Sep. Purif. Technol. 20 (2000) 1–13.

[22] A.I. Skoulidas, T.C. Bowen, C.M. Doelling, J.L. Falconer, R.D. Noble, D.S. Sholl, Comparing atomistic simulations and experimental measurements for CH4/CF4 mixture permeation through silicalite membranes, J. Membr. Sci. 227 (2003) 123–136.

[23] R. Krishna, R. Baur, Modelling issues in zeolite based separation processes, Sep. Purif. Technol. 33 (2003) 213–254.

[24] R. Krishna, R. Baur, On the Langmuir–Hinshelwood formulation for zeolite catalysed reactions, Chem. Eng. Sci. 60 (2005) 1117–1126.
[25] C. Tunca, D.M. Ford, A transition-state theory approach to adsorbate dynamics at arbitrary loadings, J. Chem. Phys. 111 (1999) 2751–2760.
[26] E. Beerdsen, D. Dubbeldam, B. Smit, Molecular simulation of loading dependent slow diffusion in confined systems, Phys. Rev. Lett. 93 (24) (2005) (Art. No. 248301).
[27] D.A. Reed, G. Ehrlich, Surface diffusion, atomic jump rates and thermodynamics, Surf. Sci. 102 (1981) 588–609.
[28] R. Krishna, D. Paschek, R. Baur, Modelling the occupancy dependence of diffusivities in zeolites, Micropor. Mesopor. Mater. 76 (2004) 233–246.
[29] A.I. Skoulidas, D.S. Sholl, Molecular dynamics simulations of self, corrected, and transport diffusivities of light gases in four silica zeolites to assess influences of pore shape and connectivity, J. Phys. Chem. A 107 (2003) 10132–10141.
[30] D.S. Sholl, Predicting single-component permeance through macroscopic zeolite membranes from atomistic simulations, Ind. Eng. Chem. Res. 39 (2000) 3737–3746.
[31] T.J.H. Vlugt, R. Krishna, B. Smit, Molecular simulations of adsorption isotherms for linear and branched alkanes and their mixtures in silicalite, J. Phys. Chem. B 103 (1999) 1102–1118.
[32] R. Krishna, B. Smit, Exploiting entropy to separate alkane isomers, Chem. Innov. 31 (1) (2001) 27–33.
[33] B. Smit, T.L.M. Maesen, Commensurate freezing of alkanes in the channels of a zeolite, Nature 374 (1995) 42–44.
[34] R. Krishna, J.M. van Baten, D. Dubbeldam, On the inflection in the concentration dependence of the Maxwell–Stefan diffusivity of CF4 in MFI zeolite, J. Phys. Chem. B 108 (2004) 14820–14822.
[35] R. Krishna, J.M. van Baten, Kinetic Monte Carlo simulations of the loading dependence of diffusion in zeolites, Chem. Eng. Technol. 28 (2005) 160–167.
[36] R. Krishna, J.M. van Baten, Influence of isotherm inflection on the diffusivities of C5-C8 linear alkanes in MFI zeolite, Chem. Phys. Lett. 407 (2005) 159–165.
[37] D. Schuring, A.O. Koriabkina, A.M. de Jong, B. Smit, R.A. van Santen, Adsorption and diffusion of *n*-hexane/2-methylpentane mixtures in zeolite silicalite: experiments and modeling, J. Phys. Chem. B 105 (2001) 7690–7698.